Available online at www.sciencedirect.com

ScienceDirect

Advances in Space Research 61 (2018) 705–714

ADVANCES IN SPACE RESEARCH (a COSPAR publication)

www.elsevier.com/locate/asr

A study of a long duration B9 flare-CME event and associated shock

R. Chandra [a,*], P.F. Chen [b], A. Fulara [a], A.K. Srivastava [c], W. Uddin [d]

[a] Department of Physics, DSB Campus, Kumaun University, Nainital 263 001, India
[b] School of Astronomy & Space Science, Nanjing University, Nanjing 210023, China
[c] Department of Physics, Indian Institute of Technology (BHU), Varanasi 221 005, India
[d] Aryabhatta Research Institute of Observational Sciences, Manora Peak, Nainital 263 001, India

Received 5 June 2017; received in revised form 17 October 2017; accepted 22 October 2017
Available online 31 October 2017

Abstract

We present and discuss here the observations of a small long duration GOES B-class flare associated with a quiescent filament eruption, a global EUV wave and a CME on 2011 May 11. The event was well observed by the Solar Dynamics Observatory (SDO), GONG Hα, STEREO and Culgoora spectrograph. As the filament erupted, ahead of the filament we observed the propagation of EIT wave fronts, as well as two flare ribbons on both sides of the polarity inversion line (PIL) on the solar surface. The observations show the co-existence of two types of EUV waves, i.e., a fast and a slow one. A type II radio burst with up to the third harmonic component was also associated with this event. The evolution of photospheric magnetic field showed flux emergence and cancellation at the filament site before its eruption.

Keywords: EUV waves; Filaments; Magnetic field; Magnetic reconnection; Coronal mass ejections (CMEs)

1. Introduction

Solar flares are the most energetic phenomenon near the solar surface and occasionally they are accompanied by filament (or prominence) eruptions and coronal mass ejections (CMEs) (Chen, 2011; Fletcher et al., 2011; Joshi et al., 2012; Benz, 2017). The association of filament eruptions with solar flares varies from small GOES B-class flares to very large GOES X-class flares. Filaments are dense cool plasma materials suspended in the hot corona (Parenti, 2014). They are often visible **at** chromospheric and coronal heights. Observations indicate that they are along the polarity inversion line (PIL). The processes related to the flare occurrence, the formation of flare ribbons, and the eruption of filament are well explained by standard CSHKP model (Carmichael, 1964; Sturrock, 1966; Hirayama, 1974; Kopp and Pneuman, 1976).

Sometimes solar flares along with erupting filaments are accompanied by globally propagating waves, known as extreme ultraviolet (EUV) waves. EUV waves were first observed by the Extreme Ultraviolet Imaging Telescope (EIT, Delaboudinière et al. (1995)) on-board the SOHO spacecraft, and were thus historically named as EIT waves (Thompson et al., 1999, 2000). These EUV waves can propagate to long distances on the solar disk with a speed of about 170–350 km s^{-1} (Thompson et al., 1999). Now, with the high cadence SDO data, our knowledge on EUV waves is enhanced considerably. EIT waves were initially considered as the coronal counterpart of high speed Chromospheric Moreton waves (Moreton, 1960), although it was also noticed that the EIT wave speeds are several times smaller than those of Moreton waves.. Later on,

* Corresponding author.
E-mail address: rchandra.ntl@gmail.com (R. Chandra).

https://doi.org/10.1016/j.asr.2017.10.034
0273-1177/

Warmuth et al. (2004) and Vršnak et al. (2016) explained that the difference in the velocities can be attributed to the deceleration of coronal waves.

The interpretations for the EUV waves include wave and non-wave models. The wave models interpret EUV waves as fast-mode MHD waves (Thompson et al., 2000; Wang, 2000). The observations like reflection, refraction, transmission seem to support the wave nature of EUV waves (Olmedo et al., 2012). The discovery of stationary fronts (Delannée and Aulanier, 1999) of EUV waves challenged the wave nature of EUV waves. Later on several other models have been proposed which include the magnetic field-line stretching model (Chen et al., 2002, 2005), the successive reconnection model (Attrill et al., 2007), the slow-mode wave model (Wills-Davey et al., 2007; Wang et al., 2009), and the current shell model (Delannée et al., 2008). The magnetic field line stretching model further proposed that there should be a fast-mode wave ahead of the slow EUV wave. It is believed in the above discussed observations and models that the slow wave stops at the magnetic quasi-separatrix layers (QSLs) and forms stationary fronts. However, very recently Chandra et al. (2016) found the observation of stationary fronts associated with the fast component of EUV waves and their location also lies at the QSLs. Encouraged by this observational finding, Chen et al. (2016) did a numerical simulation of the interaction of a fast mode MHD wave and a magnetic QSL. Their numerical results showed that the fast-mode MHD wave does generate a stationary front once passing through a magnetic QSL. Their study suggested that some part of this fast-mode wave is converted to a slow mode wave which gets trapped and forms a stationary front. Recently, this type of stationary waves is confirmed by the studies of Yuan et al. (2016), Srivastava et al. (2016), Zong and Dai (2017).

Solar flares, filament eruptions, and EUV waves are sometimes associated with type II radio bursts. Type II radio bursts are the signature of shock waves propagating in the corona. Type II radio bursts are slowly drifting radio emission from high to low frequencies (Wild and McCready, 1950). Both the EUV waves and type II radio bursts are often associated with CMEs. These type II radio bursts are believed to be triggered by either a CME (Cliver et al., 1999; Gopalswamy et al., 2001) or by a blast wave which gets created by a flare (Uchida, 1974; Hudson and Warmuth, 2004). It is difficult to determine whether a shock is ignited by a CME or a flare. Vasanth et al. (2011) studied the characteristics of type II radio bursts associated with flares and CMEs and concluded that some parts of the high frequency shocks are initiated by flares, whereas low frequency type II bursts are related to the shocks driven by CMEs. Also, Gopalswamy (1999) did a study of type II radio bursts and CMEs and suggested that at the height of minimum Alfvén speed a type II radio burst starts and the end time will depend on the relative variation of the CME speed and the Alfvén speed of the background corona.

The aim of this paper is to study the flare, filament eruption and their association with EUV waves, CME and type II radio bursts on 2011 May 11. The paper is organized as follows: Section 2 describes the observations and in Section 3, we present the analysis and results of the study. Finally in Section 4, we summarize our study.

2. Observations

For the current study, we used the data from the following sources:

- **SDO/AIA and HMI data:** The Atmospheric Imaging Assembly (AIA, (Lemen et al., 2012)) on board Solar Dynamic Observatory (SDO, Pesnell et al. (2012)) observes the full Sun with different filters in EUV and UV spectral lines. The cadence is 12 s and the pixel size is 0.6 arcsec. For this study, we used the AIA 171 Å, 193 Å, 211 Å, and 335 Å data. In order investigate the magnetic causes of the filament eruption and the associated flare, we used the data from the Heliospheric Magnetic Images (HMI, (Scherrer et al., 2012)) observations. HMI observes the photospheric magnetic field of the Sun with a cadence of 45 s and spatial resolution 1″ (i.e., the pixel size is 0.5″).
- **NSO/GONG data:** For the chromospheric observations of the filament eruption and flare, we used the Hα data from the National Solar Observatory (NSO)/ Global Oscillation Network Group (GONG, (Harvey et al., 2011)) instrument. GONG observes the full Sun in Hα with a cadence of 1 min. The spatial resolution of the GONG data is 2″ (i.e., the pixel size is 1″).
- **STEREO, LASCO, and Radio spectrograph data:** To look into the associated CME with the filament eruption, we used the COR1, COR2 (Kaiser et al., 2008) and LASCO (Brueckner et al., 1995) CME data. For the radio analysis, we used the Culgoora spectrograph data.

3. Analysis and results

3.1. Overview of the event and EUV wave

On 2011 May 11 the filament under study was located between the active regions *NOAA 11207* and *NOAA 11205* at *N20W60* on the solar disk. Earlier, this filament eruption was studied by Chandra et al. (2016) and Grechnev et al. (2015) analyzed the same event and came to the conclusion that the shock was impulsively excited by the erupting filament, which was a flux-rope progenitor, and not by the flare. The shock appeared when the CME was not yet formed. Chandra et al. (2016) reported that the eruption was associated with two global EUV waves, which were predicted by Chen et al. (2002). In their study, apart from the traditional stationary EUV front which

propagates slowly in the early phase and then stops a magnetic separatrix, they reported for the first time that the coronal fast-mode EUV wave also generates a stationary front close to another QSL. They interpretated that the magnetic structure near the stationary front could be a magnetic valley, where a part of the fast-mode wave is trapped. Later on, Chen et al. (2016) did a 2D numerical simulation and found that the stationary front results from the fast coronal wave and is located close to a magnetic QSL, which are consistent with the observations of Chandra et al. (2016). Their analysis indicates that at the place where plasma beta is equal to unity, a part of the fast-mode wave is converted into a slow-mode MHD wave. The converted slow MHD wave cannot cross the magnetic loops and forms a stationary wave front. It has been known that when a fast-mode wave enters the site with weak magnetic field where the Alfvén speed is similar to the sound speed, a part of the fast-mode wave can be converted to a slow-mode wave (Cally, 2005; McLaughlin and Hood, 2006).

The evolution of the fast and slow EUV waves shows multi-wavelength characteristics. Fig. 1 shows both the waves appearing in the AIA 335 Å, 211 Å, 193 Å, and 171 Å channels. As we can see, the waves are promptly visible in AIA 193 Å, which is a historical wavelength where EIT waves were discovered. In Table 1, we present the chronology of the event.

Table 1
Chronology of event.

Time in UT	Event
02:10	Onset of the filament eruption
02:20	Onset of the GOES B-Class flare
02:23	Onset of the EIT wave
02:25	Onset of the CME
02:28	Culgoora type II radio burst appearance
02:28	Shock onset time
02:43	Culgoora type II third harmonic appearance

3.2. Filament eruption and flare dynamics

On 2011 May 11 there were two end-to-end filaments, viz., northern and southern. The southern filament was very big, its length was around 150 Mm, while the northern filament was smaller (with a length of ≈60 Mm). In this study, we concentrate on the big southern filament, which erupted later on. First, we determine the handedness of this filament based on the definition of Mackay et al. (2010). We identify the end points of the filament and the associated magnetic polarity. The northern endpoint is found to be rooted at the positive polarity, while the south end

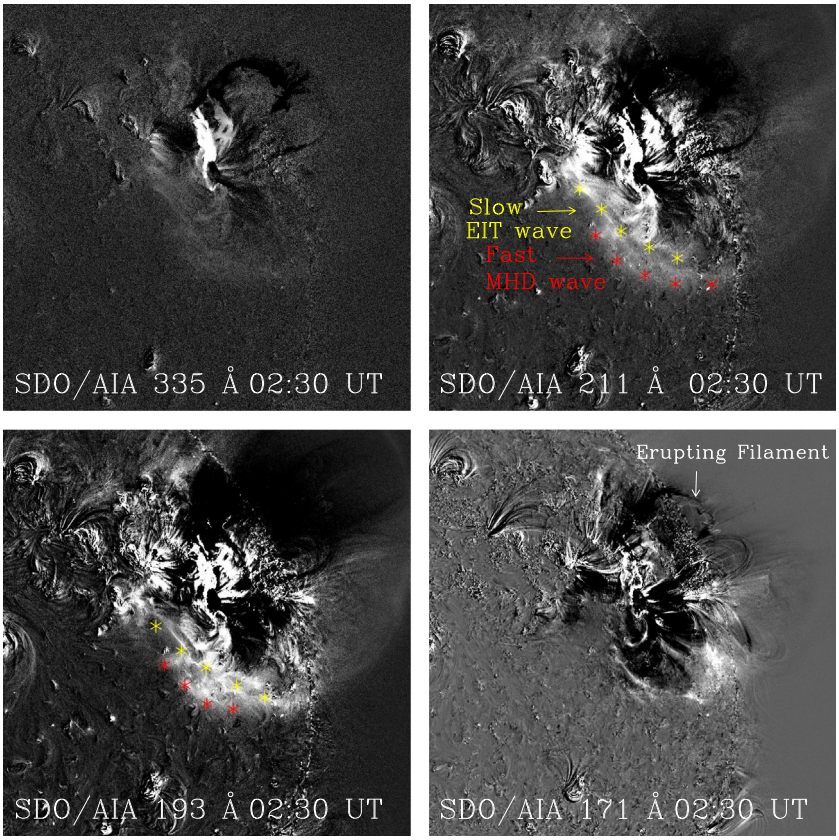

Fig. 1. A snapshot of the slow and fast EUV waves visible in different AIA wavelengths. The fast and slow waves are indicated by red and yellow asterisks, respectively. (For interpretation of the references to colour in this figure legend, the reader is referred to the web version of this article.)

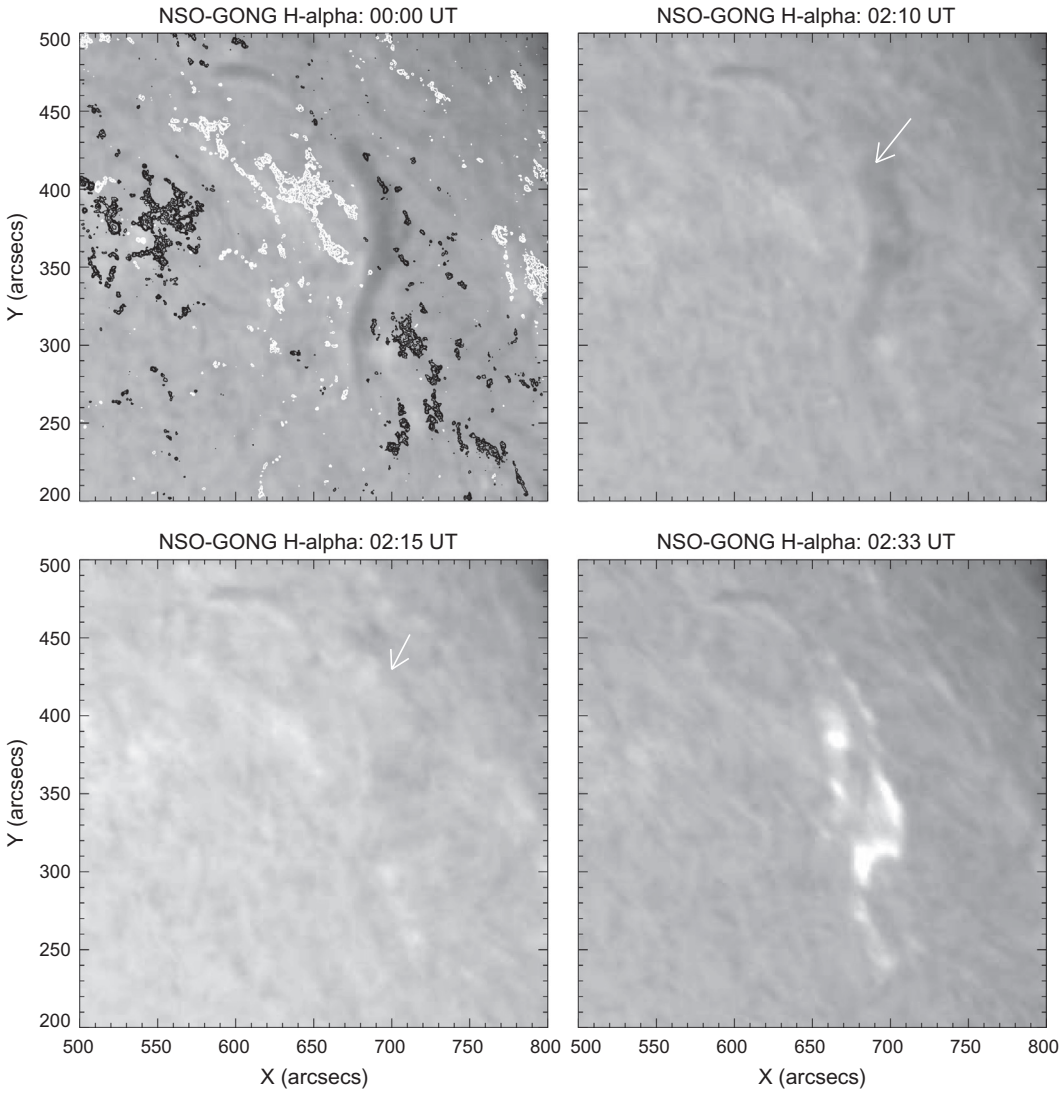

Fig. 2. Evolution of the filament eruption followed by a flare observed by NSO/GONG in Hα. The first image is overlaid by HMI magnetic field contours, where white/black contours correspond to positive/negative polarities, respectively.

is rooted at the negative polarity. The corresponding Hα filtergram overlaid by HMI magnetic field contours is presented in the first image of Fig. 2. Based on the the magnetic polarities of the two end-points of the filament, we found the filament has dextral chirality, i.e. left-handedness. According to Hao et al. (2016), the above-mentioned method sometimes does not work well. In order to confirm the result, we also determine the chirality of the filament by two other independent methods, i.e., filament barbs (Martin et al., 2008) and the drainage sites of the erupting filament (Chen et al., 2014). Looking at the barbs of the filaments, we can also see the dextral barbs, which indicates that the filament has left handedness. After checking the skew of the conjugate drainage sites in EUV wavelength, we also come to the result that the filament has left handedness. The left hand handedness confirms the hemispheric rule Pevtsov et al. (1995), Ouyang et al. (2017).

The filament started to rise at ≈02:10 UT on 2011 May 11. The eruption of the filament was recorded by *AIA* in all its channels and by *GONG* in Hα. As the filament was erupting, in *AIA* 171 Å at 02:25:13 UT, we observed the flux rope. The twist of this formed flux rope is consistent with the handedness of the filament visible in Hα wavelength.

The eruption of the filament was followed by a small *GOES* B-class flare. According to *GOES* observations, the flare was classified as B9.0-class. It was initiated around 02:20 UT, peaked 02:40 UT and decayed after 03:20 UT. The *GOES* temporal evolution of the flare is shown in Fig. 3 (top panel). In the GOES profile, we notice three peaks. The first peak was ≈02:10 UT and the second and third peak were around 02:45 and 03:05 UT, respectively. The first peak could be the pre-flare brightening as observed in the literature (Chifor et al., 2007; Joshi et al.,

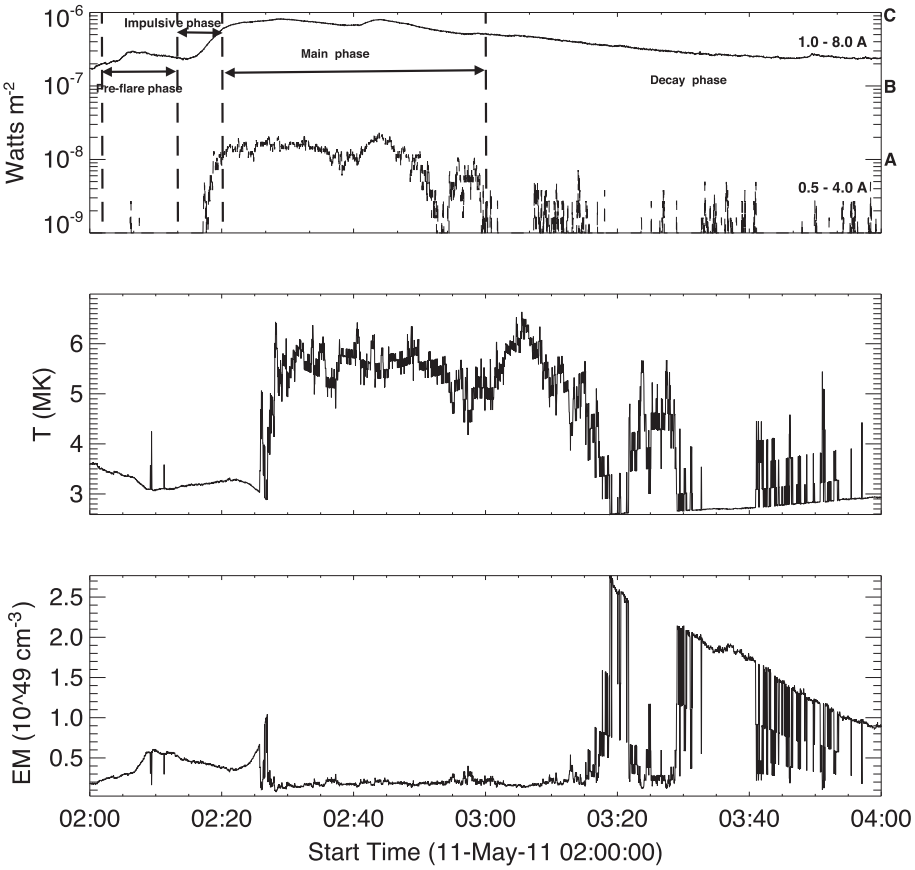

Fig. 3. Evolution of the soft X-ray flux of the flare observed by GOES (top) and the evolution of temperature (middle) and emission measure (bottom).

2011; Awasthi et al., 2014; Joshi et al., 2016). Interestingly, the time of the first peak is consistent with the start time of filament eruption. We have also computed the temperature and emission measure during the flare using GOES data. The results of this is shown in Fig. 3 (middle and bottom panel). The value of the temperature during the peak flare phase is around 6 MK. During the pre-flare phase, a small rise in the emission measure is also noticed. We noticed the anomaly in the estimation of emission measure during the period ~ 02:27–03:10 UT. Since this calculation is based on the filter-ratio method. As we discussed the flares is very small i.e. GOES B-class and the intensity is very low in GOES channels. Therefore the low GOES intensity could be responsible for the anomaly in emission measure estimation.

Looking at the spatial evolution of the flare in *AIA* 171, 304 Å as well as in GONG/Hα, the flare presented two parallel ribbons. As the filament was moving up, the two ribbons started to separate from each other, as expected by the standard CHSKP model. The ribbons are located on the opposite sides of the PIL. The ribbon structures have a reverse 'J' shape and they were shifted along the PIL. The 'J'-shaped flare ribbons were first modelled by Démoulin et al. (1996) and **were** later on were confirmed in several observations (Chandra et al., 2009; Schrijver et al., 2011; Aulanier et al., 2012; Zhao et al., 2016). Very recently,Joshi et al. (2017) reported the observations of 'J'-shaped flare ribbons in the impulsive phase of the flare. The 'J'-shaped ribbons are indicative of magnetic shear. The sign of shear depends on the shape of the ribbons: If the shape looks like a forward/reverse 'J', this represents positive/negative twist of the erupting flux rope, respectively. Therefore, in our case the **twist of the erupting flux rope** is negative, which is consistent with the chirality of the erupting filament. The evolution of the filament eruption and the flare observed by *AIA* and *GONG* is shown in Figs. 1 and 2, respectively.

3.3. CME and driven shock wave

The filament eruption was associated with a CME. The CME appeared in the LASCO field-of-view around 02:48 UT (Fig. 4, bottom panel). The CME was a partial halo event with an angular width of 225°. The speed and the acceleration of the CME are 740 km s^{-1} and 3.3 m s^{-2}, respectively. The CME is observed by the COR1 coronagraph aboard the *STEREO* twin spacecraft (A and B). *STEREO*/COR1 observes the inner corona with a field-of-view of 1.5–4$R_{\odot}$. The evolution of the CME observed by the *STEREO*/COR1 coronagraph is displayed in the top and middle panels of Fig. 4. In the figure, we can see a shock wave ahead of the CME, which is pointed out by

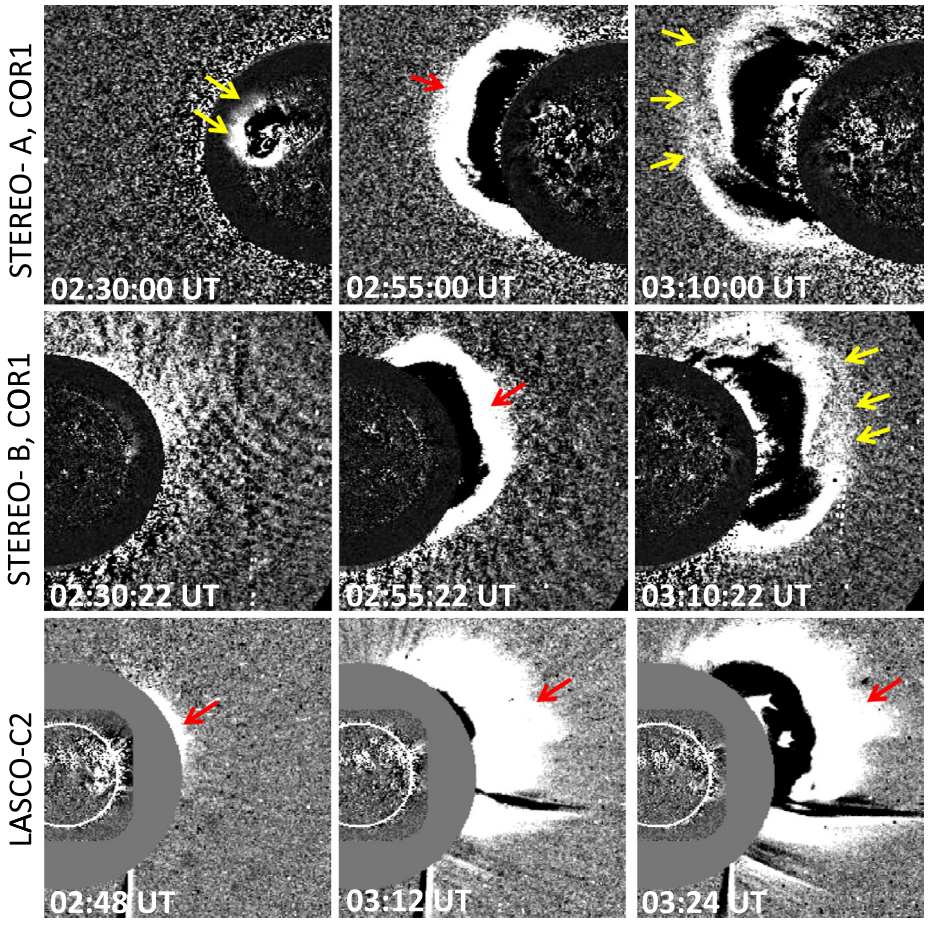

Fig. 4. Evolution of the associated CME observed by STEREO/COR1 (top and middle panels) and SOHO/LASCO C2 coronagraphs (bottom panel), respectively.

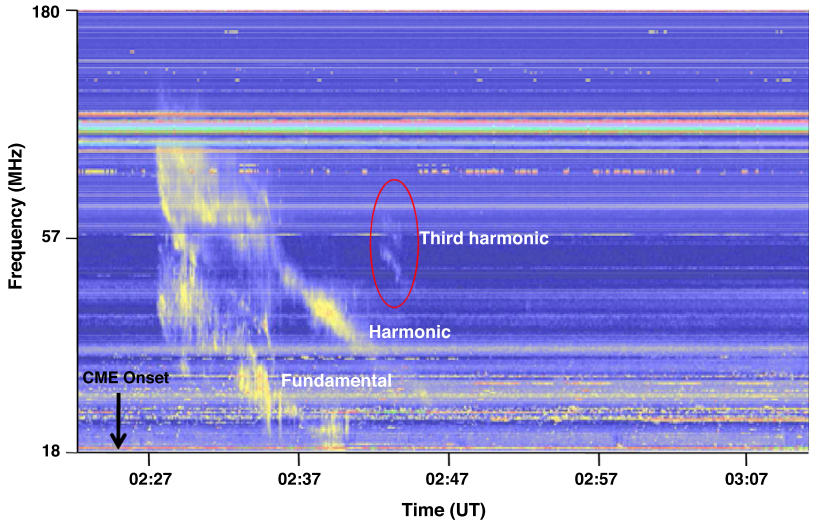

Fig. 5. The dynamic radio spectrum observed by Culgoora on 2011 May 11. The fundamental and the second harmonic components of bursts are clearly visible in the figure. The weak third harmonic is encircled.

yellow arrows, whereas the CME leading edge is marked by red arrows. The bright core embedded in the cavity is generally believed to be the erupting filament.

The filament eruption is also associated with type II radio bursts. The existence of the type II radio bursts confirms the presence of a shock. Fig. 5 displays the

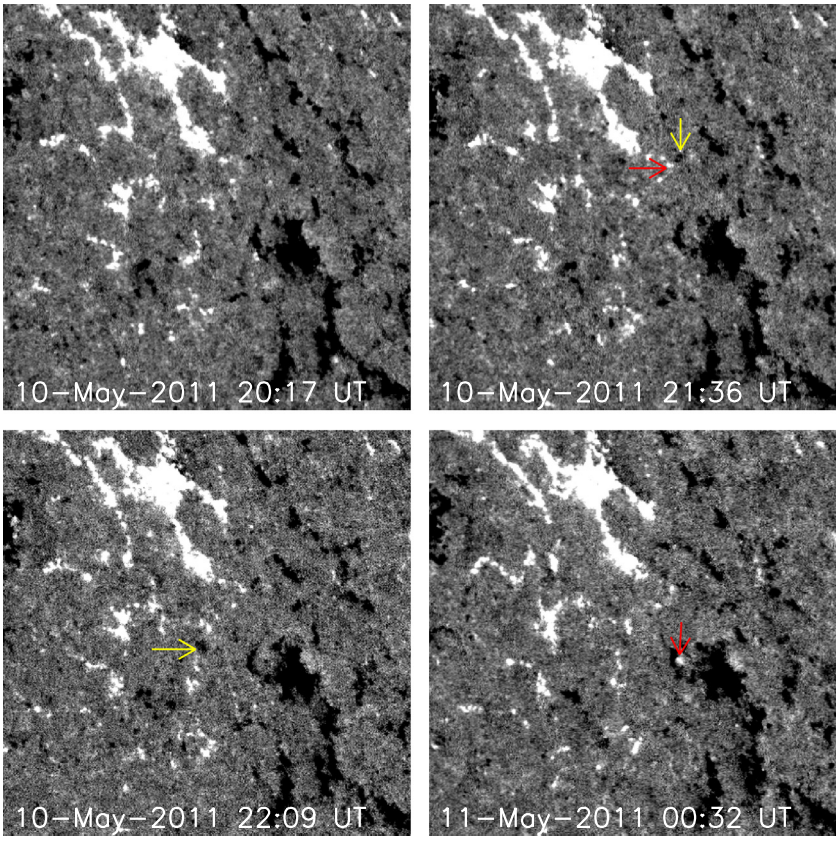

Fig. 6. Evolution of the photospheric magnetic field at the filament location. The red and yellow arrows indicate the sites of positive and negative flux emergence. (For interpretation of the references to colour in this figure legend, the reader is referred to the web version of this article.)

radio dynamic spectrum observed by the Culgoora spectrograph. It is seen that radio bursts started from 02:28 UT, when type III bursts and type II bursts were intermingled. Only after 02:36 UT, the type II radio bursts stand out clearly, which clearly show the fundamental (F) and the harmonic (H) bands. We also observed the third harmonic component, as marked by the red ellipse in Fig. 5. The observation of the third harmonic is unusual and has been reported in only a few observations in the past (Kliem et al., 1992; Zlotnik et al., 1998). The third harmonic component is split into two parallel sub-bands (see Fig. 5). Such band-splitting can be seen in the F and H bands in many events, but not in this event. The two parallel sub-bands are the consequence of the plasma emission from the upstream and the downstream sides of the shock wave (Smerd et al., 1974). These upstream and downstream sub-bands are called f_U (upper frequency branch, UFB) and f_L (lower frequency branch, LUF), respectively (Vršnak et al., 2002). Recently, Zucca et al. (2014) studied the eruption of the 2013 November 06 CME event, and they also observed two parallel lanes in the harmonic component of the type II radio bursts. They also measured the position of the type II radio source using the Nancay Radioheliograph (NRH, Kerdraon and Delouis (1997)) data at different times and frequencies. They found that the type II burst source was located above the leading edge of the CME, supporting the idea that the shock is driven by the CME.

Following Vršnak et al. (2001, 2002), in the case of low plasma β, we can calculate the Alfvén Mach number, M_A, as follows:

$$M_A = \sqrt{\frac{X(X+5)}{2(4-X)}}, \tag{1}$$

where $X = (f_U/f_L)^2$. From Fig. 5, the values of f_U and f_L are 57 MHz and 45.3 MHz, respectively. The resulting Mach number is derived to be 1.46, which is in accordance with previously reported values (Zucca et al., 2014; Vršnak et al., 2002; Nindos et al., 2011; Su et al., 2015).

3.4. Evolution of photospheric magnetic field

As described above, the 2011 May 11 event was associated with the eruption of a quiescent filament. To understand the triggering of the filament eruption, we investigated the evolution of the photospheric magnetic field near the filament location. Some snapshots of the magnetic field before the filament eruption are presented in Fig. 6. The filament was exactly located along a PIL. We observed positive and negative flux emergence at several places inside the filament channel before the filament eruption. The emerging positive and negative polarities

are indicated by red and yellow arrows, respectively (see also the attached movie). Afterwards, some of them started to cancel and finally fully canceled. According to Feynman and Martin (1995) and Chen and Shibata (2000), the emergence of reconnection-favoring magnetic flux near a filament channel can trigger the eruption of the filament. From the above discussion, we believe that the filament eruption is due to the flux emergence and cancellation inside the filament channel. It is possible that due to this flux emergence and cancellation, the flux rope loses its equilibrium, and started to rise.

4. Summary

In this study, we presented the multi-wavelength observations of a GOES B-class flare occurring on 2011 May 11. The main results of our study are summarized as follows:

- The observed GOES B9 flare has prolonged soft X-ray emission for more than an hour (from 02:20 UT to 03:20 UT) with multiple peaks. The event shows a pre-flare phase from $\sim$ 02:00 to $\sim$ 02:20 UT with a peak at $\sim$ 02:10 UT.
- The flare is also associated with almost all the other eruptive phenomena, such as a filament eruption, a CME, EUV waves, and type II radio bursts. Therefore this event presents an excellent example in which we could see all the eruptive phenomena simultaneously.
- Before the filament eruption, we observed flux emergence and cancellation, which could be responsible for the triggering of the filament eruption.
- The event shows that a part of the fast-mode MHD EUV wave stops at the magnetic QSL, which can be explained by mode conversion, i.e., a part of the fast-mode wave is converted to a slow-mode wave..
- We observed the third harmonic component of the associated type II radio bursts, which is an unusual phenomenon.

Acknowledgments

We are grateful to the reviewers for their constructive comments and suggestions. The authors thank the SDO, STEREO, SOHO, Culgoora, and GONG teams for the open data policy. PFC was supported by the Chinese foundation (NSFC 11533005) and Jiangsu 333 Project.

References

Attrill, G.D.R., Harra, L.K., van Driel-Gesztelyi, L., Démoulin, P., 2007. Coronal "Wave": magnetic footprint of a coronal mass ejection? ApJL 656, L101–L104. https://doi.org/10.1086/512854.

Aulanier, G., Janvier, M., Schmieder, B., 2012. The standard flare model in three dimensions. I. Strong-to-weak shear transition in post-flare loops. A & A 543, A110. https://doi.org/10.1051/0004-6361/201219311.

Awasthi, A.K., Jain, R., Gadhiya, P.D., Aschwanden, M.J., Uddin, W., Srivastava, A.K., Chandra, R., Gopalswamy, N., Nitta, N.V., Yashiro, S., Manoharan, P.K., Choudhary, D.P., Joshi, N.C., Dwivedi, V.C., Mahalakshmi, K., 2014. Multiwavelength diagnostics of the precursor and main phases of an M1.8 flare on 2011 April 22. MNRS 437, 2249–2262. https://doi.org/10.1093/mnras/stt2032.

Benz, A.O., 2017. Flare observations. Living Rev. Sol. Phys. 14, 2–60. https://doi.org/10.1007/s41116-016-0004-3.

Brueckner, G.E., Howard, R.A., Koomen, M.J., Korendyke, C.M., Michels, D.J., Moses, J.D., Socker, D.G., Dere, K.P., Lamy, P.L., Llebaria, A., Bout, M.V., Schwenn, R., Simnett, G.M., Bedford, D.K., Eyles, C.J., 1995. The Large Angle Spectroscopic Coronagraph (LASCO). Sol. Phys. 162, 357–402. https://doi.org/10.1007/BF00733434.

Cally, P.S., 2005. Local magnetohelioseismology of active regions. MNRAS 358, 353–362. https://doi.org/10.1111/j.1365-2966.2005.08742.x.

Carmichael, H. 1964, A Process for Flares in The Physics of Solar Flares, Hess, W.N., (ed.), NASA Special Publication vol. 50, pp. 451–456.

Chandra, R., Chen, P.F., Fulara, A., Srivastava, A.K., Uddin, W., 2016. Peculiar stationary EUV wave fronts in the eruption on 2011 May 11. ApJ 822, 106–113. https://doi.org/10.3847/0004-637X/822/2/106.

Chandra, R., Schmieder, B., Aulanier, G., Malherbe, J.M., 2009. Evidence of magnetic helicity in emerging flux and associated flare. Sol. Phys. 258, 53–67. https://doi.org/10.1007/s11207-009-9392-z.

Chen, P.F., 2011. Coronal mass ejections: models and their observational basis. Living Rev. Sol. Phys. 8, 1–92. https://doi.org/10.12942/lrsp-2011-1.

Chen, P.F., Fang, C., Chandra, R., Srivastava, A.K., 2016. Can a fast-mode EUV wave generate a stationary front? Sol. Phys. 291, 3195–3206. https://doi.org/10.1007/s11207-016-0920-3.

Chen, P.F., Fang, C., Shibata, K., 2005. A full view of EIT waves. ApJ 622, 1202–1210. https://doi.org/10.1086/428084.

Chen, P.F., Harra, L.K., Fang, C., 2014. Imaging and spectroscopic observations of a filament channel and the implications for the nature of counter-streamings. ApJ 784, 50–58. https://doi.org/10.1088/0004-637X/784/1/50.

Chen, P.F., Shibata, K., 2000. An emerging flux trigger mechanism for coronal mass ejections. ApJ 545, 524–531. https://doi.org/10.1086/317803.

Chen, P.F., Wu, S.T., Shibata, K., Fang, C., 2002. Evidence of EIT and Moreton waves in numerical simulations. ApJL 572, L99–L102. https://doi.org/10.1086/341486.

Chifor, C., Tripathi, D., Mason, H.E., Dennis, B.R., 2007. X-ray precursors to flares and filament eruptions. A & A 472, 967–979. https://doi.org/10.1051/0004-6361:20077771.

Cliver, E.W., Webb, D.F., Howard, R.A., 1999. On the origin of solar metric type II bursts. Sol. Phys. 187, 89–114. https://doi.org/10.1023/A:1005115119661.

Delaboudinière, J.P., Artzner, G.E., Brunaud, J., Gabriel, A.H., Hochedez, J.F., Millier, F., Song, X.Y., Au, B., Dere, K.P., Howard, R.A., Kreplin, R., Michels, D.J., Moses, J.D., Defise, J.M., Jamar, C., Rochus, P., Chauvineau, J.P., Marioge, J.P., Catura, R.C., Lemen, J. R., Shing, L., Stern, R.A., Gurman, J.B., Neupert, W.M., Maucherat, A., Clette, F., Cugnon, P., van Dessel, E.L., 1995. EIT: extreme-ultraviolet imaging telescope for the SOHO mission. Sol. Phys. 162, 291–312. https://doi.org/10.1007/BF00733432.

Delannée, C., Aulanier, G., 1999. Cme associated with transequatorial loops and a bald patch flare. Sol. Phys. 190, 107–129. https://doi.org/10.1023/A:1005249416605.

Delannée, C., Török, T., Aulanier, G., Hochedez, J.F., 2008. A new model for propagating parts of EIT Waves: a current shell in a CME. Sol. Phys. 247, 123–150. https://doi.org/10.1007/s11207-007-9085-4.

Démoulin, P., Priest, E.R., Lonie, D.P., 1996. Three-dimensional magnetic reconnection without null points 2. Appllication to twisted flux tubes. JGR 101, 7631–7646. https://doi.org/10.1029/95JA03558.

Feynman, J., Martin, S.F., 1995. The initiation of coronal mass ejections by newly emerging magnetic flux. JGR 100, 3355–3367. https://doi.org/10.1029/94JA02591.

Fletcher, L., Dennis, B.R., Hudson, H.S., Krucker, S., Phillips, K., Veronig, A., Battaglia, M., Bone, L., Caspi, A., Chen, Q., Gallagher, P., Grigis, P.T., Ji, H., Liu, W., Milligan, R.O., Temmer, M., 2011. An observational overview of solar flares. SSR 159, 19–106. https://doi.org/10.1007/s11214-010-9701-8.

Gopalswamy N., 1999, X-ray and microwave signatures of coronal mass ejections. In: Proceedings of the Nobeyama Symposium, vol. 479, pp. 141–152.

Gopalswamy, N., Yashiro, S., Kaiser, M.L., Howard, R.A., Bougeret, J. L., 2001. Characteristics of coronal mass ejections associated with long-wavelength type II radio bursts. JGR 106, 29219–29230. https://doi.org/10.1029/2001JA000234.

Grechnev, V.V., Uralov, A.M., Kuzmenko, I.V., Kochanov, A.A., Chertok, I.M., Kalashnikov, S.S., 2015. Responsibility of a filament eruption for the initiation of a flare, CME, and blast wave, and its possible transformation into a bow shock. Sol. Phys. 290, 129–158. https://doi.org/10.1007/s11207-014-0621-8.

Hao, Q., Guo, Y., Fang, C., Chen, P.F., Cao, W.D., 2016. Can we determine the filament chirality by the filament footpoint location or the barb-bearing? Res. Astron. Astrophys. 16, 1–12. https://doi.org/10.1088/1674-4527/16/1/001.

Harvey J.W., Bolding J., Clark R., Hauth D., Hill F., Kroll R., Luis G., Mills N., Purdy T., Henney C., Holland D., Winter J., 2011. Full-disk solar H-alpha images from GONG. In: AAS/Solar Physics Division Abstracts #42, Bulletin of the American Astronomical Society, vol. 43, pp.17–45.

Hirayama, T., 1974. Theoretical model of flares and prominences. Sol. Phys. 34, 323–337. https://doi.org/10.1007/BF00153671.

Hudson, H.S., Warmuth, A., 2004. Coronal loop oscillations and flare shock waves. ApJL 614, L85–L88. https://doi.org/10.1086/425314.

Joshi, B., Veronig, A.M., Lee, J., Bong, S.-C., Tiwari, S.K., Cho, K.-S., 2011. Pre-flare activity and magnetic reconnection during the evolutionary stages of energy release in a solar eruptive flare. ApJ 743, 195–207. https://doi.org/10.1088/0004-637X/743/2/195.

Joshi, B., Veronig, A.M., Manoharan, P.K., Somov, V., 2012. Signatures of magnetic reconnection in solar eruptive flares: a multi-wavelength perspective. Astrophys. Space Sci. Proc. 33, 29–41.

Joshi, B., Kushwaha, U., Veronig, A.M., Cho, K.-S., 2016. Pre-flare coronal jet and evolutionary phases of a solar eruptive prominence associated with the M1.8 Flare: SDO and RHESSI observations. ApJ 832, 130–144. https://doi.org/10.3847/0004-637X/832/2/130.

Joshi, B., Kushwaha, U., Veronig, A.M., Dhara, S.K., Shanmugaraju, A., Moon, Y.-J., 2017. Formation and eruption of a flux rope from the sigmoid active region NOAA 11719 and associated M6.5 flare: a multi-wavelength study. ApJ 834, 42–57. https://doi.org/10.3847/1538-4357/834/1/42.

Kaiser, M.L., Kucera, T.A., Davila, J.M., St. Cyr, O.C., Guhathakurta, M., Christian, E., 2008. The STEREO mission: an introduction. SSR 136, 5–16. https://doi.org/10.1007/s11214-007-9277-0.

Kerdraon, A., Delouis, J.-M., 1997. Coronal physics from radio and space observations. In: Proceedings of the CESRA Workshop, vol. 483, pp. 193–201. doi:https://doi.org/10.1007/BFb0106448.

Kliem, B., Krueger, A., Treumann, R.A., 1992. Third plasma harmonic radiation in type II bursts. Sol. Phys. 140, 149–160. https://doi.org/10.1007/BF00148435.

Kopp, R.A., Pneuman, G.W., 1976. Magnetic reconnection in the corona and the loop prominence phenomenon. Sol. Phys. 50, 85–98. https://doi.org/10.1007/BF00206193.

Lemen, J.R., Title, A.M., Akin, D.J., Boerner, P.F., Chou, C., Drake, J. F., Duncan, D.W., Edwards, C.G., Friedlaender, F.M., Heyman, G. F., Hurlburt, N.E., Katz, N.L., Kushner, G.D., Levay, M., Lindgren, R.W., Mathur, D.P., McFeaters, E.L., Mitchell, S., Rehse, R.A., Schrijver, C.J., Springer, L.A., Stern, R.A., Tarbell, T.D., Wuelser, J. P., Wolfson, C.J., Yanari, C., Bookbinder, J.A., Cheimets, P.N., Caldwell, D., Deluca, E.E., Gates, R., Golub, L., Park, S., Podgorski, W.A., Bush, R.I., Scherrer, P.H., Gummin, M.A., Smith, P., Auker, G., Jerram, P., Pool, P., Soufli, R., Windt, D.L., Beardsley, S., Clapp, M., Lang, J., Waltham, N., 2012. The Atmospheric Imaging Assembly (AIA) on the Solar Dynamics Observatory (SDO). Sol. Phys. 275, 17–40. https://doi.org/10.1007/s11207-011-9776-8.

Mackay, D.H., Karpen, J.T., Ballester, J.L., Schmieder, B., Aulanier, G., 2010. Physics of solar prominences: II magnetic structure and dynamics. SSR 151, 333–399. https://doi.org/10.1007/s11214-010-9628-0.

Martin, S.F., Lin, Y., Engvold, O., 2008. A method of resolving the 180-degree ambiguity by employing the chirality of solar features. Sol. Phys. 250, 31–51. https://doi.org/10.1007/s11207-008-9194-8.

McLaughlin, J.A., Hood, A.W., 2006. MHD mode coupling in the neighbourhood of a 2D null point. A & A 459, 641–649. https://doi.org/10.1051/0004-6361:20065558.

Moreton, G.E., 1960. Hα observations of flare-initiated disturbances with velocities ~1000 km/sec. ApJ 65, 494–495. https://doi.org/10.1086/108346.

Nindos, A., Alissandrakis, C.E., Hillaris, A., Preka-Papadema, P., 2011. On the relationship of shock waves to flares and coronal mass ejections. A & A 531, A31. https://doi.org/10.1051/0004-6361/201116799.

Olmedo, O., Vourlidas, A., Zhang, J., Cheng, X., 2012. Secondary waves and/or the "Reflection" from and "Transmission" through a coronal hole of an extreme ultraviolet wave associated with the 2011 February 15 X2.2 flare observed with SDO/AIA and STEREO/EUVI. ApJ 756, 143–155. https://doi.org/10.1088/0004-637X/756/2/143.

Ouyang, Y., Zhou, Y.H., Chen, P.F., Fang, C., 2017. Chirality and magnetic configurations of solar filaments. ApJ 835, 94–102. https://doi.org/10.3847/1538-4357/835/1/94.

Parenti, S., 2014. Solar prominences: observations. Living Rev. Sol. Phys. 11, 1–88. https://doi.org/10.12942/lrsp-2014-1.

Pesnell, W.D., Thompson, B.J., Chamberlin, P.C., 2012. The Solar Dynamics Observatory (SDO). Sol. Phys. 275, 3–15. https://doi.org/10.1007/s11207-011-9841-3.

Pevtsov, A.A., Canfield, R.C., Metcalf, T.R., 1995. Latitudinal variation of helicity of photospheric magnetic fields. ApJL 440, L109–L112. https://doi.org/10.1086/187773.

Scherrer, P.H., Schou, J., Bush, R.I., Kosovichev, A.G., Bogart, R.S., Hoeksema, J.T., Liu, Y., Duvall, T.L., Zhao, J., Title, A.M., Schrijver, C.J., Tarbell, T.D., Tomczyk, S., 2012. The Helioseismic and Magnetic Imager (HMI) investigation for the Solar Dynamics Observatory (SDO). Sol. Phys. 275, 207–227. https://doi.org/10.1007/s11207-011-9834-2.

Schrijver, C.J., Aulanier, G., Title, A.M., Pariat, E., Delannée, C., 2011. The 2011 February 15 X2 flare, ribbons, coronal front, and mass ejection: interpreting the three-dimensional views from the solar dynamics observatory and stereo guided by magnetohydrodynamic flux-rope modeling. ApJ 738, 167–189.167. https://doi.org/10.1088/0004-637X/738/2/167.

Smerd, S.F., Sheridan, K.V., Stewart, R.T., 1974. On split-band structure in type II radio bursts from the sun (presented by S.F. Smerd). In: Newkirk, G.A. (Ed.) Coronal Disturbances, IAU Symposium, 57, Dordrecht, Reidel, Boston, pp. 389–393.

Srivastava, A.K., Singh, T., Ofman, L., Dwivedi, B.N., 2016. Inference of magnetic field in the coronal streamer invoking kink wave motions generated by multiple EUV waves. MNRAS 463, 1409–1415. https://doi.org/10.1093/mnras/stw2017.

Sturrock, P.A., 1966. Model of the high-energy phase of solar flares. Nature 211, 695–697. https://doi.org/10.1038/211695a0.

Su, W., Cheng, X., Ding, M.D., Chen, P.F., Sun, J.Q., 2015. A type II radio burst without a coronal mass ejection. ApJ 804, 88–96. https://doi.org/10.1088/0004-637X/804/2/88.

Thompson, B.J., Gurman, J.B., Neupert, W.M., Newmark, J.S., Delaboudinière, J.P., Cyr, O.C.S., Stezelberger, S., Dere, K.P., Howard, R.A., Michels, D.J., 1999. SOHO/EIT observations of the 1997 April 7 coronal transient: possible evidence of Coronal Moreton waves. ApJL 517, L151–L154. https://doi.org/10.1086/312030.

Thompson, B.J., Reynolds, B., Aurass, H., Gopalswamy, N., Gurman, J. B., Hudson, H.S., Martin, S.F., St. Cyr, O.C., 2000. Observations of the 24 September 1997 Coronal Flare waves. Sol. Phys. 193, 161–180. https://doi.org/10.1023/A:1005222123970.

Uchida, Y., 1974. Behavior of the flare produced coronal MHD wavefront and the occurrence of type II radio bursts. Sol. Phys. 39, 431–449. https://doi.org/10.1007/BF00162436.

Vasanth, V., Umapathy, S., Vršnak, B., Anna Lakshmi, M., 2011. Characteristics of type-II radio bursts associated with flares and CMEs. Sol. Phys. 273, 143–162. https://doi.org/10.1007/s11207-011-9854-y.

Vršnak, B., Aurass, H., Magdalenić, J., Gopalswamy, N., 2001. Band-splitting of coronal and interplanetary type II bursts. I. Basic properties. A & A 377, 321–329. https://doi.org/10.1051/0004-6361:20011067.

Vršnak, B., Magdalenić, J., Aurass, H., Mann, G., 2002. Band-splitting of coronal and interplanetary type II bursts. II. Coronal magnetic field and Alfvén velocity. A & A 396, 673–682. https://doi.org/10.1051/0004-6361:20021413.

Vršnak, B., Žic, T., Lulić, S., Temmer, M., Veronig, A.M., 2016. Formation of Coronal large-amplitude waves and the chromospheric response. Sol. Phys. 291, 89–115. https://doi.org/10.1007/s11207-015-0822-9.

Wang, H., Shen, C., Lin, J., 2009. Numerical experiments of wave-like phenomena caused by the disruption of an unstable magnetic configuration. ApJ 700, 1716–1731. https://doi.org/10.1088/0004-637X/700/2/1716.

Wang, Y.M., 2000. EIT waves and fast-mode propagation in the solar corona. ApJL 543, L89–L93. https://doi.org/10.1086/318178.

Warmuth, A., Vršnak, B., Magdalenić, J., Hanslmeier, A., Otruba, W., 2004. A multiwavelength study of solar flare waves. I. Observations and basic properties. A & A 418, 1101–1115. https://doi.org/10.1051/0004-6361:20034332.

Wild, J.P., McCready, L.L., 1950. Observations of the spectrum of high-intensity solar radiation at metre wavelengths. I. The apparatus and spectral types of solar burst observed. Aust. J. Sci. Res. A Phys. Sci. 3, 387–398. https://doi.org/10.1071/PH500387.

Wills-Davey, M.J., DeForest, C.E., Stenflo, J.O., 2007. Are "Are EIT Waves" fast-mode MHD waves? ApJ 664, 556–562. https://doi.org/10.1086/519013.

Yuan, D., Li, B., Walsh, R.W., 2016. Secondary fast magnetoacoustic waves trapped in randomly structured plasmas. ApJ 828, 17–21. https://doi.org/10.3847/0004-637X/828/1/17.

Zhao, J., Gilchrist, S.A., Aulanier, G., Schmieder, B., Pariat, E., Li, H., 2016. Hooked flare ribbons and flux-rope-related QSL footprints. ApJ 823, 62–71. https://doi.org/10.3847/0004-637X/823/1/62.

Zlotnik, E.Y., Klassen, A., Klein, K.L., Aurass, H., Mann, G., 1998. Third harmonic plasma emission in solar type II radio bursts. A & A 331, 1087–1098.

Zong, W., Dai, Y., 2017. Mode conversion of a solar extreme-ultraviolet wave over a coronal cavity. ApJL 834, L15–L20. https://doi.org/10.3847/2041-8213/834/2/L15.

Zucca, P., Pick, M., Démoulin, P., Kerdraon, A., Lecacheux, A., Gallagher, P.T., 2014. Understanding coronal mass ejections and associated shocks in the solar corona by merging multiwavelength observations. ApJ 795, 68–72. https://doi.org/10.1088/0004-637X/795/1/68.